Kinetic Monte Carlo Simulations of Nucleation and Growth in Electrodeposition

Lian Guo, Aleksandar Radisic, and Peter C. Searson*

Department of Materials Science and Engineering, Johns Hopkins University, Baltimore, Maryland 21218

Received: September 8, 2005; In Final Form: October 25, 2005

Nucleation and growth during bulk electrodeposition is studied using kinetic Monte Carlo (KMC) simulations. Ion transport in solution is modeled using Brownian dynamics, and the kinetics of nucleation and growth are dependent on the probabilities of metal-on-substrate and metal-on-metal deposition. Using this approach, we make no assumptions about the nucleation rate, island density, or island distribution. The influence of the attachment probabilities and concentration on the time-dependent island density and current transients is reported. Various models have been assessed by recovering the nucleation rate and island density from the current−time transients.

Introduction

Deposition of metals on foreign metal substrates often occurs through Volmer−Weber island growth. In thin film deposition, the evolution of film morphology is determined in large part by nucleation and growth, and hence, understanding the details of these processes for different systems is critically important. For example, the minimum thickness for a continuous film, d_{crit}, is determined by the island density N. For hemispherical islands, it can be shown that $d_{crit} \approx N^{-1/2}$; thus, an island density on the order of 10^{12} cm^{-2} is required to obtain a continuous thin film of 10 nm. With the increasing use of electrodeposition in conjunction with lithography and other patterning techniques, feature sizes less than 100 nm are common, and hence, nucleation and growth are increasingly important in the fabrication of nanoscale structures.

Although the mechanism of overpotential deposition has been widely studied over the past 50 years, there is still considerable controversy over even the most basic principles of nucleation and growth, as indicated in a recent review paper.[1] For the case of diffusion-limited growth, the difficulty in modeling comes from the competition for ions between adjacent islands. By introducing of the concept of diffusion zones and applying the Avrami theorem to account for overlap, Scharifker and Hills derived an analytical model (SH model)[2,3] for nucleation followed by diffusion-limited growth of hemispherical islands. Two limiting cases are considered for nucleation. Instantaneous nucleation corresponds to the case where nucleation is sufficiently fast that all islands are formed before substantial growth has occurred, and hence, $N(t) = N_0$, where N_0 is the nucleus density In progressive nucleation, the nucleus density increases linearly with time, $N(t) = k_n N_0 t$, where k_n is the nucleation rate constant. The SH model is widely used by experimentalists to analyze deposition current transients from which parameters such as the island density or nucleation rate can be extracted.

Subsequently, there have been several modifications of the SH model, most of which have addressed the method for treating the diffusion zones. Scharifker and Mostany[4] (SM) reported a general version of the SH model, allowing both the nucleation rate and the island density to be extracted from transient analysis. Sluyters-Rehbach, Wijenberg, Bosco, and Sluyters[5] (SRWBS) implemented a more general expression for nucleation and treated diffusion zone overlap in a slightly different way. Heerman and Tarallo[6] reconciled the SM and SRWBS models by building the diffusion layer thickness as a function of the nucleation rate constant and obtained an expression identical to the rate law derived earlier by Mirkin and Nilov[7] (MN). Cao et al.[8] used numerical simulations to solve the diffusion equation and avoid making any assumptions about the overlap of diffusion zones. Using a random distribution of nuclei, the transients obtained from the numerical simulations showed reasonable agreement with the SH, MN, and SWRBS models for instantaneous nucleation, but significant differences were seen for progressive nucleation, especially at longer times.

Surprisingly, there have been very few simulation studies of multiple-site nucleation followed by 3D diffusion-limited growth. Sharifker et al.[9] performed 2D simulations using the diffusion zone concept to compare the SM model with the SRWBS model. Nagy et al.[10,11] implemented simulations to study the growth of a single hemispherical island using Brownian dynamics to model the ions in solution. Fransaer and Penner[12] addressed the size dispersion of islands during instantaneous nucleation followed by 3D diffusion-limited growth using Brownian dynamics. Simulation current transients showed good agreement with the SH model at low island density, although substantial deviations were observed at large island densities because of the overlap of the diffusion zones at short times.

A common feature of all of these models and simulations are that they are growth models based on a priori assumptions about the nucleation rate or the nucleus density and distribution. In addition, the details of the attachment process are usually ignored because the islands are considered hemispherical and the addition of an atom simply increments the radius. These constraints are particularly important because the limitations of the existing models have become apparent only recently as experimentalists have investigated parameters such as the time dependence of the island density. In many cases, experimentally determined current transients show reasonable agreement with existing models; however, parameters such as the nucleation rate and island density are often in significant disagreement with experimentally determined values.[13,14] This is especially prevalent at high island densities, which are of particular practical interest.

In this article, we report on kinetic Monte Carlo (KMC) simulations of nucleation and growth during the early stages of

* To whom correspondence should be addressed. E-mail: searson@jhu.edu.

10.1021/jp055077u CCC: $30.25
Published on Web 11/30/2005

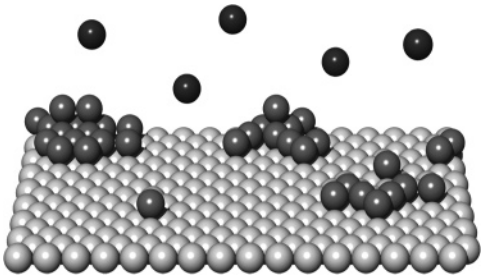

Figure 1. Schematic illustration of simulations. Metal ions in the bulk solution are governed by Brownian dynamics. Metal atoms deposited on the surface are immobile because there is no surface diffusion or dissolution.

overpotential deposition. Because we make no assumptions about the island density, island distribution, or nucleation rate, we are able to explore the relationship between the deposition current and island nucleation and growth.

Simulation Method

Simulations were performed using the kinetic Monte Carlo method.[15] Here, we explore the case of deposition of a metal M onto a substrate S with no surface diffusion. Figure 1 shows a schematic illustration of the simulations. In the solution, metal ions are modeled as point charges that undergo random walks. Initially, ions are randomly distributed in the simulation volume at a given bulk concentration. In each time step, all ions are moved a distance λ at a random azimuthal angle. The displacement λ corresponds to the mean free path for the metal ion in aqueous solution at room temperature and is taken as 2 times the hydrodynamic diameter.[16] After all of the ions in solution have been moved, the elapsed time increases by τ, which can be deduced from the Einstein−Smoluchowski equation

$$D = \frac{\lambda^2}{6\tau} \tag{1}$$

where D is the diffusion coefficient.

A metal ion whose trajectory intersects the surface can be electrochemically reduced to form a metal atom either on the substrate or on a growing metal island. The probability that a metal ion is reduced directly onto the substrate is denoted as P_{M-S}, and the probability that a metal ion is reduced to a metal atom on a growing island is denoted as P_{M-M}. It is evident that Volmer−Weber island growth occurs when $P_{M-S} < P_{M-M}$. Macroscopically, this is equivalent to the case where the rate of reduction onto the substrate is lower than the rate of reduction onto the same metal. The use of deposition probabilities is convenient because the equilibrium potential for a redox couple consisting of metal ions and a foreign metal substrate (M^{n+}/S) cannot be defined. The relationship between the attachment probabilities and the applied potential can be inferred from a comparison of the dependence on parameters such as the island density and nucleation rate.

Defining different probabilities or rate constants for metal-on-substrate and metal-on-metal deposition is particularly important in exploring the interplay between nucleation and growth. The difference in rates gives rise to the so-called nucleation overpotential in systems where the onset of metal deposition on a foreign metal substrate occurs at more negative potentials than the onset of deposition on the same metal substrate.

The substrate in our simulations is a face-centered-cubic (fcc) (111) surface. For convenience, depositing metal atoms are allowed to occupy only fcc lattice sites. This condition means that all islands have the same crystal orientations perpendicular and parallel to the substrate plane.

As described above, P_{M-S} represents the probability that a metal ion is reduced to a metal atom on the substrate to form an adatom. Because we do not allow the back reaction to occur (we assume that the potential is sufficiently far from the equilibrium potential) and because there is no surface diffusion, the critical nucleus size is effectively one atom. We note that a critical nucleus size of one has been deduced for several systems.[17−21] The reduction of a metal ion to form an adatom on the substrate can occur at any available fcc lattice site, i.e., one-half of the 3-fold hollow sites on a given (111) plane. Thus, the simulations make no assumptions about the location or distribution of nucleation sites. We note that all of the models described above begin by assuming a nucleus distribution or a nucleation rate and then determine the rate expressions for the growth process.

In our simulations, we make no assumptions about whether the deposition is kinetically or diffusion-limited. If the sticking probabilities are sufficiently large, then ions will be depleted in the vicinity of growing islands, and the deposition reaction becomes diffusion-limited. Conversely, if the sticking probabilities are sufficiently low, the deposition reaction becomes kinetically limited.

For the simulations reported here, $P_{M-M} = 10^{-2}-1$, and P_{M-S} is varied between 10^{-6} and 10^{-2}. In this range of probabilities, deposition is diffusion-limited. The time increment in the simulations is determined by the diffusion coefficient and mean free path for ions in solution and hence represents real time. The deposition current is simply determined from the number of atoms that are deposited per unit time. The simulation runtimes on a Dell Precision Workstation 450 with dual CPUs were about one week for the smallest values of the deposition probabilities.

For the simulations reported here, we use values of λ, D, and a (lattice parameter) for copper. The hydrodynamic diameter for copper ions is 0.370 nm,[16] resulting in a mean free path of 0.74 nm. For copper(II) in aqueous solution, we take $D = 6 \times 10^{-6}$ cm^2 s^{-1}.[22] From the lattice parameter for fcc Cu, the near-neighbor spacing is 0.255 nm. The rectangular substrate size was between 128 × 128 (33 nm × 28 nm) and 512 × 512 (131 nm × 113 nm). Periodic boundary conditions were applied in the lateral directions. The height of the simulation box was 800−2000 lattice sites depending on the simulation runtime. In all cases, it was verified that the ion concentration at the top of the box was not depleted at the end of the simulation. It was also verified that the island density was independent of the substrate size, i.e., there were no finite-size effects. Each simulation was repeated 10−1000 times, depending on the values of P_{M-S} and P_{M-M}, to achieve statistically meaningful results. All current−time transients and island density−time curves represent the averages of multiple runs.

Results and Discussion

Figure 2 shows a series of current−time transients for deposition from a 71 mM solution with $P_{M-M} = 1$ and metal-on-substrate deposition probabilities P_{M-S} from $10^{-5}-10^{-2}$. The deposition transients show an initial increase in current followed by a decrease at longer times. These features are characteristic of nucleation and growth where the initial current is due to diffusion-limited growth of individual noninteracting islands and the current decrease at longer times is due to overlap of the diffusion fields resulting in planar diffusion to the growing islands. The transients exhibit a characteristic current maximum i_{max} at time t_{max}.

Figure 3 shows a series of plan-view images for deposition with $P_{M-M} = 1$ and $P_{M-S} = 10^{-3}$. At $t = 0.5 \times 10^{-6}$ s, the

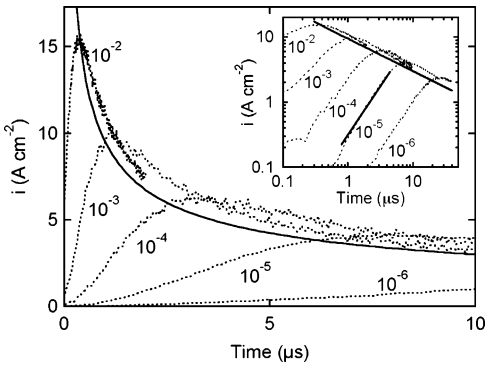

Figure 2. Deposition current versus time obtained from simulations with $P_{M-M} = 1$ and a metal ion concentration of 71 mM. Values of P_{M-S} are indicated in the figure. The solid line corresponds to the Cottrell equation. The inset shows a double logarithmic plot of the same data. The solid line above corresponds to the Cottrell equation. The solid line below gives the slope of $^3/_2$.

islands are relatively small with a density $N(t) \approx 1.5 \times 10^{12}$ cm^{-2}. As deposition proceeds, islands formed at earlier times grow, and new islands are formed, resulting in a broadening of the size distribution. Because there is no surface diffusion in these simulations, all islands have an irregular shape. In the image at 1×10^{-6} s, close to t_{max}, the island density clearly increases. At longer times, there is little change in the island density although the islands increase in size.

Plots of the island density versus time obtained from analysis of the simulation images along with the corresponding deposition transients are shown in Figure 4. At short times, the island density increases linearly with time. At long times, approximately corresponding to $1.2t_{max}$, the island density saturates.

Nucleation in electrodeposition is usually considered in the following way. As described previously, N_0 is the final nucleus density, and $N(t)$ is the nucleus density at time t; hence, $N_0 - N(t)$ represents the density of unoccupied nucleation sites. Assuming that the rate of nucleation is dependent on the density of unoccupied sites, we can write $dN(t)/dt = k_n[N_0 - N(t)]$, where k_n is the nucleation rate constant. Integration gives

$$N(t) = N_0[1 - \exp(-k_n t)] \qquad (2)$$

The integration constant $C = -\ln(N_0)$ is determined from the condition that $N(t) = 0$ at $t = 0$. Two limiting cases can be identified from this equation. If k_n is sufficiently large so that $k_n t \gg 1$ and $t \ll t_{max}$, then $N(t) = N_0$. Conversely, if k_n is sufficiently small so that $k_n t \ll 1$ at short times, then $N(t) = k_n N_0 t$, and the density of nuclei increases linearly with time. In electrochemistry, these two cases correspond to instantaneous nucleation and progressive nucleation, respectively.

Fits of the time dependence of the island density using eq 2 are shown in Figure 4. In all cases, there is good agreement between the simple first-order nucleation model and the island density obtained from the simulation images. The $N(t)$ versus t curves for the different attachment probabilities can be compared by plotting the normalized island density N/N_0 versus t/t_{max}. Figure 5 shows that the nucleation rate is approximately constant ($k_n t \ll 1$) up to about $0.8t_{max}$. The fact that the nucleation rate naturally evolves to follow the progressive nucleation model provides a foundation for comparison to existing rate laws.

Having demonstrated that the island density is consistent with progressive nucleation up to $0.8t_{max}$, we can compare the current−time transients to the SH model. For progressive nucleation, the time-dependent deposition current density (normalized to the geometric surface area) is given by[2,3]

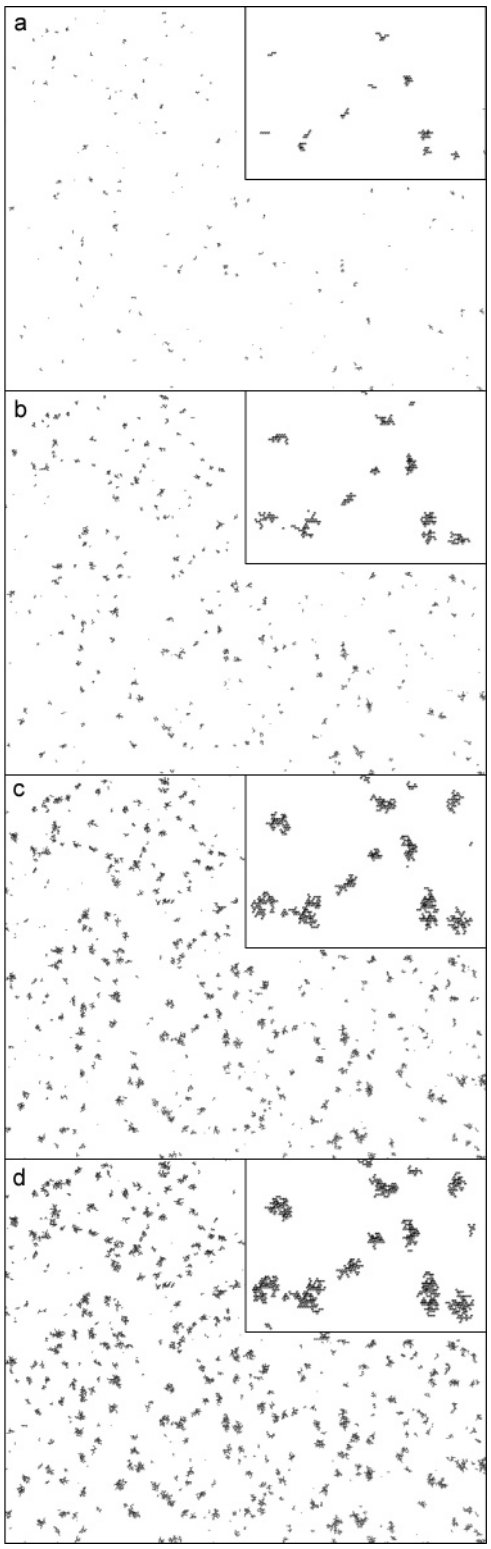

Figure 3. Plan-view images of deposition for $P_{M-M} = 1$ and $P_{M-S} = 10^{-3}$ in 71 mM solution after (a) 0.5×10^{-6}, (b) 1×10^{-6} , (c) 2×10^{-6}, and (d) 3×10^{-6} s. The area is 30 nm × 24 nm. The insets show higher-magnification images of the simulations.

$$i(t) = \frac{zFcD^{1/2}}{\pi^{1/2}t^{1/2}}\left\{1 - \exp\left[-\frac{2}{3}k_n N_0 D(8\pi^3 c V_m)^{1/2}t^2\right]\right\} \qquad (3)$$

where c is the bulk concentration, D is the diffusion coefficient, z is the valence of the metal ion ($z = 2$ for copper), F is

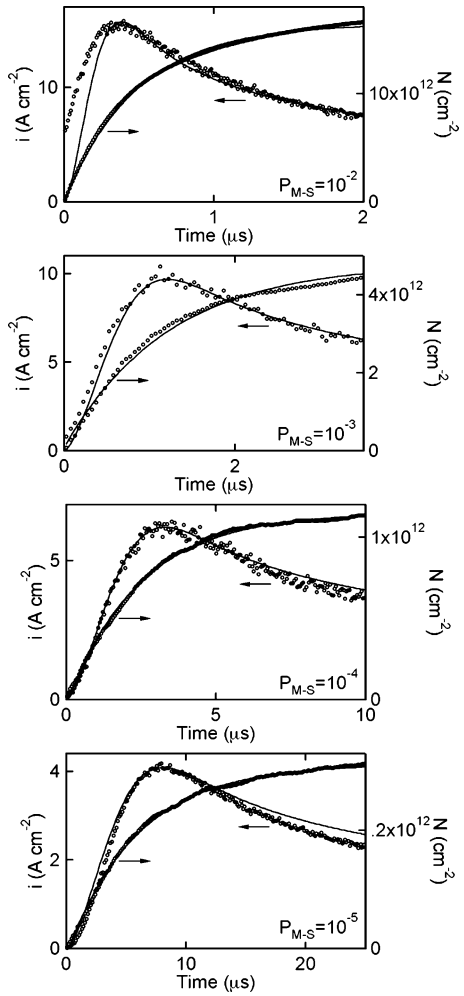

Figure 4. Deposition current and island density versus time for $P_{M-M} = 1$ and $P_{M-S} = 10^{-2}$, 10^{-3}, 10^{-4}, and 10^{-5}. The solid lines on the deposition transients show fits to the SH model using the values for i_{max} and t_{max} determined from Figure 2. The solid lines on the island density curves correspond to fits to eq 2. The metal ion concentration was 71 mM.

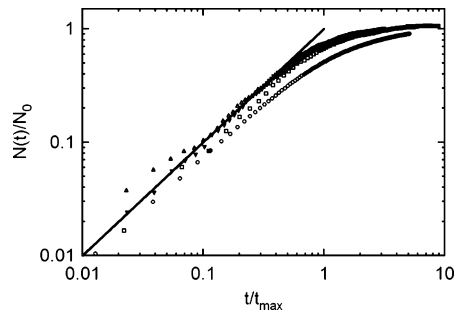

Figure 5. log N/N_0 versus log t/t_{max} for $P_{M-M} = 1$ and $P_{M-S} =$ (○) 10^{-2}, (□) 10^{-3}, (△) 10^{-4}, and (▽) 10^{-5}.

Faraday's constant, V_m is the molar volume of the solid (V_m = 7.1 cm^3 mol^{-1} for copper), and k_n is the nucleation rate constant.

The solid lines superimposed on the current−time transients in Figure 4 are fits to the SH model (eq 3) using i_{max} and t_{max}. In general, the fits to the simulation results using the SH model for progressive nucleation and 3D diffusion-limited growth are very good. We note, however, that for large values of P_{M-S}, the current is higher than for the SH model for $t < t_{max}$ and for small values of P_{M-S} the current is lower than for the SH model for $t > t_{max}$.

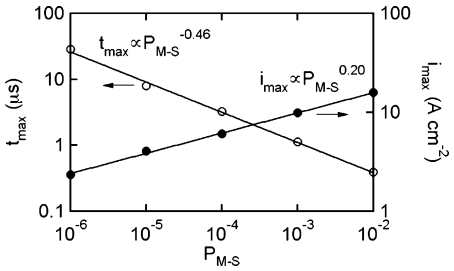

Figure 6. Dependence of i_{max} and t_{max} on attachment probability P_{M-S} for $P_{M-M} = 1$ and a metal ion concentration of 71 mM.

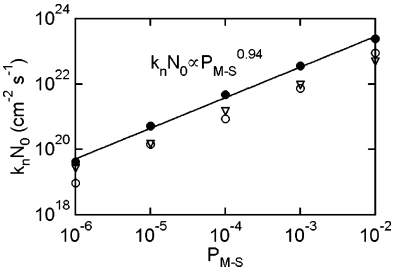

Figure 7. Dependence of the nucleation rate k_nN_0 on attachment probability P_{M-S} for $P_{M-M} = 1$ and a metal ion concentration of 71 mM.

The deviation from the SH model at short times seen for large P_{M-S} has been observed experimentally.[9,23] In the simulations, this effect is due to the partial current associated with metal ion reduction onto the substrate and decreases quickly to zero as the growing islands reduce the ion concentration at the substrate surface. This effect is not included in any models. The deviation from the SH model at long times for small overpotentials has also has been observed experimentally for copper depositing on ruthenium[24] from 50 mM $CuSO_4$ and gold deposition on n-type silicon[25] from 10 mM $KAu(CN)_2$ at low overpotential.

Figure 6 shows the dependence of the maximum current, i_{max}, and the time at which the maximum current occurs, t_{max}, on the metal-on-substrate deposition probability P_{M-S}. Both i_{max} and t_{max} exhibit a power-law dependence on P_{M-S}. From Figure 4, we obtain $i_{max} \propto P_{M-S}^{0.20}$, $t_{max} \propto P_{M-S}^{-0.46}$, and $\partial \log t_{max}/\partial \log i_{max} = -2.3$. According to the SH model for progressive nucleation followed by three-dimensional diffusion-limited growth, i_{max} and t_{max} are given by

$$i_{max} = 0.4959zFD^{3/4}(8\pi V_m)^{1/8}c^{9/8}(k_nN_0)^{1/4} \quad (4)$$

$$t_{max} = 3.318D^{-1/2}(8\pi cV_m)^{-1/4}(k_nN_0)^{-1/2} \quad (5)$$

The potential dependence of i_{max} and t_{max} appears indirectly in these expressions through the nucleation rate k_nN_0; all other terms are potential-independent. The SH model predicts $i_{max} \propto (k_nN_0)^{1/4}$, $t_{max} \propto (k_nN_0)^{-1/2}$, and $\partial \log t_{max}/\partial \log i_{max} = -2$. Thus, in evaluating the dependence of i_{max} and t_{max} on P_{M-S}, we must also take into account the dependence of k_nN_0 on P_{M-S}.

Figure 7 shows the logarithm of the nucleation rate plotted versus the logarithm of P_{M-S}. The nucleation rate k_nN_0 was determined from the fits to the island density versus time plots (Figure 4) and from the SH model. In the SH model, the nucleation rate can be determined from i_{max} and t_{max} using

$$k_nN_0 = 0.2898(8\pi cV_m)^{-1/2}\frac{(zFc)^2}{i_{max}^2 t_{max}^3} \quad (6)$$

The nucleation rate can also be determined from the current−time transient during the early stages of growth where the islands are largely noninteracting. The dependence of the current on time for progressive nucleation and growth of noninteracting islands, i.e., for $t < t_{max}$, is given by[26]

$$i = \frac{2}{3} nFk_n N_0 \pi (2Dc)^{3/2} V_m^{1/2} t^{3/2} \quad (7)$$

The inset in Figure 2 shows that the initial part of the deposition current transients for small values P_{M-S} exhibit a growth exponent of $^3/_2$, as predicted by eq 7. However, the exponent decreases with increasing P_{M-S} as a result of the increasing contribution of the metal-on-substrate current.

The nucleation rate obtained from analysis of the simulation images exhibits a power-law dependence on the metal-on-substrate deposition probability with $k_n N_0 \propto P_{M-S}^{0.94}$. From Figure 7, it is seen that the nucleation rate obtained from the SH model (eqs 6 and 7) is significantly lower than the nucleation rate $k_n N_0$ obtained independently from the simulation images.

We can now compare the simulation results in Figure 6 ($i_{max} \propto P_{M-S}^{0.20}$, $t_{max} \propto P_{M-S}^{-0.46}$) to the SH model. From the dependence of the nucleation rate on the deposition probability ($k_n N_0 \propto P_{M-S}^{0.94}$), we obtain $i_{max} \propto (k_n N_0)^{0.21}$ and $t_{max} \propto (k_n N_0)^{-0.49}$. These values are in good agreement with the SH model, which predicts that $i_{max} \propto (k_n N_0)^{0.25}$ and $t_{max} \propto (k_n N_0)^{-0.5}$. The ratio of the exponents from our simulations, $\partial \log t_{max}/\partial \log i_{max} = -2.3$, is slightly larger than the value of -2 expected from the SH model if $k_n N_0$ is the only potential-dependent parameter.

Many experimental studies of nucleation and growth during electrodeposition have shown that $k_n N_0$, i_{max}, and t_{max} are exponentially dependent on potential. Our simulations show power-law relationships between $k_n N_0$, i_{max}, and t_{max} and the attachment probability P_{M-S} (Figures 6 and 7), which implies that $U \propto \log P_{M-S}$. From experimental measurements,[17,18,27] $-\partial U/\partial \log i_{max}$ is found to be in the range 197−325 mV, and $\partial U/\partial \log t_{max}$ is 95−166 mV. Comparison to our simulations (for $P_{M-M} = 1$) implies that $-\partial U/\partial \log P_{M-S}$ is 40−76 mV. Values of $-\partial U/\partial \log(k_n N_0)$ determined from experimental measurements using the SH model are in the range 45−89 mV. Using $k_n N_0 \propto P_{M-S}^{0.94}$, we obtain $-\partial U/\partial \log P_{M-S} = 42-83$ mV, in good agreement with the values obtained from i_{max} and t_{max}. These results suggest that an order-of-magnitude increase in P_{M-S} corresponds to an increase in overpotential of about 40−80 mV.

Figure 8 shows a series of plots of the deposition current and island density versus time for different metal ion concentrations with $P_{M-M} = 1$ and $P_{M-S} = 10^{-3}$. At all four concentrations from 10 to 100 mM, the current transients maintain the same general features as described previously. With increasing concentration, i_{max} increases and t_{max} decreases. However, the increase in i_{max} is noticeably larger than the decrease in t_{max}. As described above, increasing P_{M-S} results in a decrease in t_{max} ($t_{max} \propto P_{M-S}^{-0.46}$) and a weaker increase in i_{max} ($i_{max} \propto P_{M-S}^{0.20}$). In the framework of the SH model, increasing concentration results in an increase in the diffusive flux to the growing islands and an increase in the nucleation rate. The corresponding island density versus time curves show that the nucleation rate and final island density increase with increasing bulk concentration. For all concentrations, the time evolution of the island density shows excellent agreement with eq 2.

The nucleation rate exhibits a power-law dependence on metal ion concentration with $k_n N_0 \propto c^{1.02}$, as shown in Figure 9. The concentration dependence of $k_n N_0$ is dominated by the strong concentration dependence of k_n. Experimentally, the concentration dependence of nucleation and growth has not been widely studied. Oskam[18] studied gold deposition on n-Si(100) in 0.5−50 mM $KAu(CN)_2$, and Hoffmann[17] studied copper deposition on *n*-Si(100) in 20−100 mM $Cu_2P_2O_7$. In both cases, t_{max} and $k_n N_0$ were found to be independent of concentration; however, at constant potential (where $k_n N_0$ is constant), $i_{max} \propto c^{9/8}$ as predicted by the SH model.

The dependencies of i_{max} and t_{max} on metal ion concentration in the simulations are shown in Figure 10. An increase in the ion concentration results in a higher island density, which enhances the current response by providing more sites for attachment. Similarly, the increase in the island density decreases

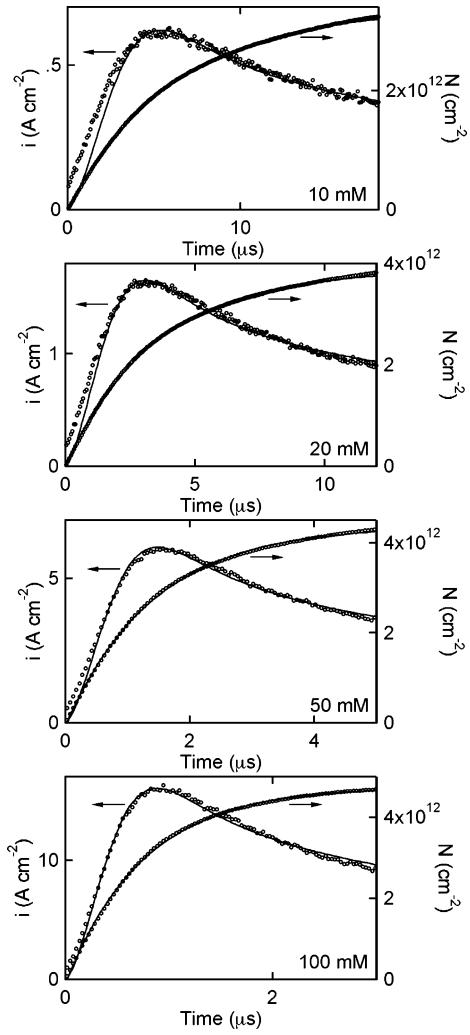

Figure 8. Deposition current and island density versus time for $P_{M-M} = 1$ and $P_{M-S} = 10^{-3}$ and a metal ion concentration of 10, 20, 50, and 100 mM.

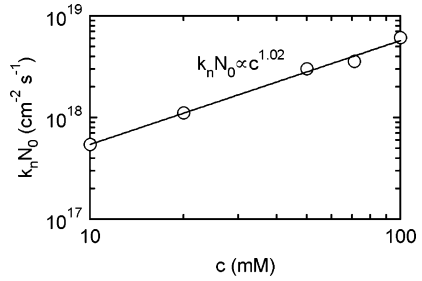

Figure 9. Dependence of the nucleation rate $k_n N_0$ on concentration for $P_{M-M} = 1$ and $P_{M-S} = 10^{-3}$. The metal ion concentration was 71 mM.

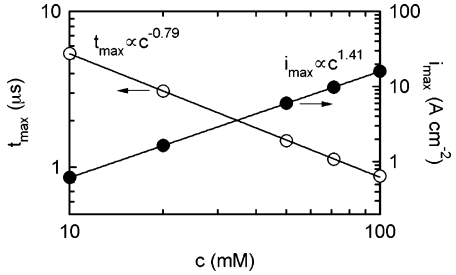

Figure 10. Dependence of i_{max} and t_{max} on metal ion concentration for $P_{M-M} = 1$ and $P_{M-S} = 10^{-3}$. The metal ion concentration was 71 mM.

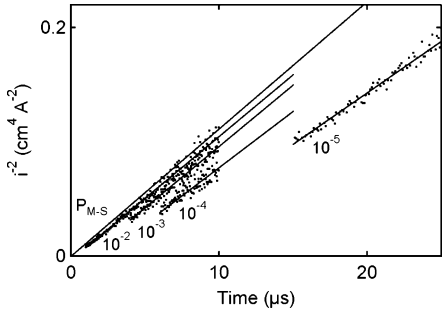

Figure 11. Plots of i^{-2} versus time ($t > t_{max}$) for different values of P_{M-S} with $P_{M-M} = 1$ and a metal ion concentration of 71 mM. The thick solid line corresponds to the Cottrell equation, and the other four lines correspond to linear least-squares fits.

t_{max} because interaction of the diffusion zones occurs at shorter times. Both parameters exhibit a power-law relation with concentration, with $i_{max} \propto c^{1.41}$ and $t_{max} \propto c^{-0.79}$. In contrast, the SH model predicts $i_{max} \propto c^{1.12}$ ($c^{9/8}$) and $t_{max} \propto c^{-0.25}$, as can be seen from eqs 4 and 5. The difference arises from the concentration dependence of k_nN_0 in the simulations, as described above. From our simulations, we obtain $k_nN_0 \propto c^{1.02}$, and taking into account that $i_{max} \propto (k_nN_0)^{0.25}$ and $t_{max} \propto (k_nN_0)^{-0.5}$, we obtain $i_{max} \propto c^{1.15}$ and $t_{max} \propto c^{-0.28}$, in excellent agreement with the SH model. These results suggest that detailed studies of the influence of concentration on nucleation are needed.

As noted above, the simulation current transients deviate from the SH model for large values of P_{M-S} and low concentrations. This effect is due to the current contribution from metal-on-substrate deposition. From simple collision theory, it is expected that the partial current due to ion reduction on the substrate should be proportional to the metal ion concentration and the probability of deposition (P_{M-S}). The initial current, $i_{t\to0}$, obtained from the simulations by extrapolating the deposition current transients to $t = 0$ is proportional to P_{M-S} and c, from which we obtain $i_{t\to0} \propto P_{M-S}^{1.0}$ and $i_{t\to0} \propto c^{1.0}$. As described above, $i_{max} \propto P_{M-S}^{0.20}$ and $i_{max} \propto c^{1.41}$. Comparison shows that $i_{t\to0}$ increases much faster than i_{max} as P_{M-S} increases and that $i_{t\to0}$ increases more slowly than i_{max} as the concentration increases. Thus, we can see that partial current due to ion reduction on the substrate is always present but is masked by the partial current due to ion reduction on the growing metal islands at low values of P_{M-S} or high concentrations.

From eq 3, it is evident that in the SH model for $t > t_{max}$, the deposition current is described by the Cottrell equation

$$i(t) = \frac{zFcD^{1/2}}{\pi^{1/2}t^{1/2}} \tag{8}$$

Figure 11 shows the deposition transients in Figure 2 replotted as i^{-2} versus t for $t > t_{max}$. All of the simulation transients exhibit good linearity; however, it is evident that the slope decreases and the intercept shifts from the origin as P_{M-S} decreases. From the slope for $P_{M-S} = 10^{-2}$, we obtain $D = 6.2 \times 10^{-6}$ cm^2 s^{-1}, very close to the value of $D = 6.0 \times 10^{-6}$ cm^2 s^{-1} used in the simulations. For $P_{M-S} = 10^{-5}$, we obtain a significantly larger value of $D = 7.3 \times 10^{-6}$ cm^2 s^{-1}. This effect is due to the fact that the diffusion layer expands more slowly as the nucleation rate decreases. The SH model (eq 3) imposes the restriction that the current is described by the Cottrell equation at long times. However, modifications of the SH model that do not impose this restriction show excellent agreement with the Cottrell equation for large k_n but increasing deviation above the Cottrell current with decreasing nucleation rate.[6] Cao et al.,[28] using numerical simulations of the diffusion equation, reported that the deposition current for progressive nucleation at $t > t_{max}$ was best described by the Cottrell equation with an offset. From Figure 2, it can be seen that the current for $t > t_{max}$ is larger than the Cottrell current and that the deviation increases with decreasing P_{M-S}. It is this deviation that gives rise to the apparent increase in diffusion coefficient.

To compare our simulations to the various models for nucleation and growth, we compare k_n and N_0 obtained from fits to our simulations to the value obtained from analysis of the simulation images. Nonlinear fitting was used to extract k_n and N_0, and the results are presented in Table 1. The relative mean square error χ^2/i_{max}^2 is given for each model. The parameter χ^2 is defined as

$$\chi^2 = \sum_i (y - y_i)^2 \tag{9}$$

where y is the fitted (model) value for a given point and y_i is the measured value for the point. As seen from eq 9, χ^2 gives the absolute deviation by summing the mean square error for all data points; thus, we use χ^2/i_{max}^2 to obtain the relative deviation. Empirically, good fits are obtained when $\chi^2/i_{max}^2 < 0.2$. From the table, it is seen that the values obtained from all three models deviate significantly from the values obtained directly from the simulation images, sometimes by as much as an order of magnitude. Of the analytical models, the values obtained for k_n and N_0 from the MN model are close to the simulation values for $P_{M-S} = 10^{-3}$ and 10^{-4}. These results demonstrate the significant errors that can result in obtaining k_n and N_0 from experimental data using the analytical models.

Figure 12 shows two deposition transients and the corresponding island density versus time curves for $P_{M-M} < 1$ with

TABLE 1: Comparison of k_n (s^{-1}) and N_0 (cm^{-2}) Obtained from the KMC Simulations Reported Here and the Values Extracted from the Simulations Using the SM, SRWBS, and MN Models

	KMC		SM model			SRWBS model			MN model		
P_{M-S}	k_n	N_0	k_n	N_0	χ^2/i_{max}^2	k_n	N_0	χ^2/i_{max}^2	k_n	N_0	χ^2/i_{max}^2
10^{-2}	1.33×10^6	1.83×10^{13}	2.00×10^7	3.63×10^{12}	1.88	1.42×10^7	3.56×10^{12}	1.91	7.74×10^6	4.12×10^{12}	1.30
10^{-3}	7.80×10^5	4.57×10^{12}	1.79×10^5	1.47×10^{13}	1.50	4.53×10^5	4.75×10^{12}	1.52	6.03×10^5	2.99×10^{12}	0.08
10^{-4}	4.07×10^5	1.15×10^{12}	1.21×10^5	2.85×10^{12}	4.53	9.71×10^4	2.67×10^{12}	4.52	9.00×10^4	2.35×10^{12}	0.14
10^{-5}	1.69×10^5	3.12×10^{11}	3.91×10^4	1.41×10^{12}	4.84	3.19×10^4	1.29×10^{12}	4.83	2.15×10^4	1.57×10^{12}	0.20
10^{-6}	5.46×10^4	7.60×10^{10}	9.64×10^3	5.55×10^{11}	6.31	8.14×10^3	4.94×10^{11}	6.32	5.21×10^3	5.53×10^{11}	0.69

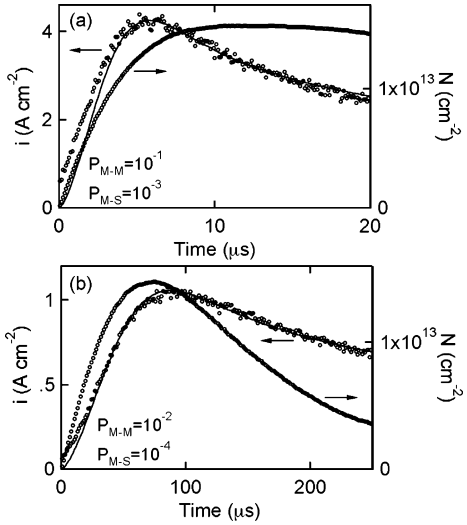

Figure 12. Deposition current and island density versus time for a metal ion concentration of 71 mM with (a) $P_{M-M} = 10^{-1}$, $P_{M-S} = 10^{-3}$ and (b) $P_{M-M} = 10^{-2}$, $P_{M-S} = 10^{-4}$.

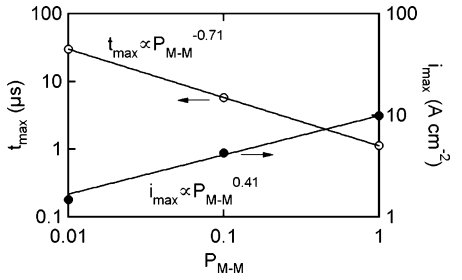

Figure 13. Dependence of i_{max} and t_{max} on the metal-on-metal attachment probability P_{M-M} for $P_{M-S} = 10^{-3}$ and a metal ion concentration of 71 mM.

$c = 71$ mM. For $P_{M-M} = 10^{-1}$ and $P_{M-S} = 10^{-3}$, the deposition transient exhibits the same general features as shown in Figure 2, consistent with nucleation and diffusion-limited growth. Comparison with the deposition transient for $P_{M-M} = 1$ and $P_{M-S} = 10^{-3}$ (Figure 4b) shows that t_{max} is considerably longer and i_{max} is considerably smaller as P_{M-M} is decreased from 1 to 0.1. We also note that the current at short times is larger than seen in Figure 4b. This effect results from the partial current due to metal-on-substrate deposition and appears to be associated with the ions competing between substrate and the nucleus. The corresponding island density decreases slightly at long times as a result of the onset of coalescence of the islands. The deposition transient for $P_{M-M} = 10^{-2}$ and $P_{M-S} = 10^{-4}$ also shows good agreement with the SH model, although the deviation at short times is smaller. The influence of island coalescence is also more significant in this case.

The relation between the metal-on-metal deposition probability P_{M-M} and the current−time response is further explored in Figure 13, where i_{max} and t_{max} are plotted versus P_{M-M}. Here, the metal-on-substrate deposition probability P_{M-S} is fixed at 10^{-3}, and the ion concentration is 71 mM. Both i_{max} and t_{max} exhibit a power-law relationship with P_{M-M} from which we obtain $i_{max} \propto {P_{M-M}}^{0.41}$ and $t_{max} \propto {P_{M-M}}^{-0.71}$. By comparison with the relations $i_{max} \propto {P_{M-S}}^{0.20}$ and $t_{max} \propto {P_{M-S}}^{-0.46}$ obtained for constant P_{M-M}, it is evident that P_{M-M} exerts more influence on the current−time transient than P_{M-S}.

The magnitudes of i_{max} reported here are somewhat larger than for typical experiments. Our ability to access typical values observed in experiments is limited by the simulation runtime; however, we can see that, for $P_{M-M} = 10^{-6}$ and $P_{M-S} = 10^{-8}$, we obtain $i_{max} \approx 5$ mA cm^{-2} and $t_{max} \approx 1$ s, close to experimental values. Nonetheless, the power-law dependences of many of the parameters allow us to infer similar behavior for smaller values of P_{M-M} and P_{M-S}. Thus, these simulations provide a valuable tool for understanding the atomic-scale details of nucleation and growth.

Summary

We have used KMC simulations of metal deposition to study nucleation and growth during the early stages of overpotential deposition. We show that, for all values of P_{M-S} and P_{M-M}, the island density follows the first-order rate law based on the density of unoccupied sites at the surface. The island density increases linearly with time (progressive nucleation) up to about $0.8t_{max}$. The current−time transients exhibit the initial increase and subsequent decrease characteristic of nucleation and diffusion-limited growth. In many cases, the transients show good agreement with the SH model. Deviations at short times are associated with large values of P_{M-S}, where the additional current due to metal-on-substrate deposition is significant. Deviations at long times are associated with small values of P_{M-S}, where the slow build up of the diffusion layer results in currents that are larger than predicted by the Cottrell equation. Comparison of the dependence of the nucleation rate on P_{M-S} with the dependence of the nucleation rate on the applied potential reported in the literature allows us to relate the attachment probability to the applied potential.

We also show that the current−time transients and nucleation rates are dependent on the metal ion concentration and the value of P_{M-M}. The concentration dependencies of i_{max} and t_{max} are similar to the predictions of the SH model. The nucleation rate exhibits a power-law dependence on P_{M-S} with an exponent of 1.02. Simulations with P_{M-M} between 10^{-2} and 1 exhibit current−time transients with similar features. Comparison of the exponents for the dependences of i_{max} and t_{max} on P_{M-M} and P_{M-S} reveals that P_{M-M} has a stronger influence on the current transients than P_{M-S}.

Acknowledgment. This work was partially supported by the National Center for Supercomputing Applications (NCSA) under Grant DMR050010N.

References and Notes

(1) Hyde, M. E.; Compton, R. G. *J. Electroanal. Chem.* **2003**, *549*, 1−12.
(2) Scharifker, B.; Hills, G. *Electrochim. Acta* **1983**, *28*, 879−889.
(3) Gunawardena, G.; Hills, G.; Montenegro, I.; Scharifker, B. *J. Electroanal. Chem.* **1982**, *138*, 225−239.
(4) Scharifker, B. R.; Mostany, J. *J. Electroanal. Chem.* **1984**, *177*, 13−23.
(5) Sluyters-Rehbach, M.; Wijenberg, J. H. O. J.; Bosco, E.; Sluyters, J. H. *J. Electroanal. Chem.* **1987**, *236*, 1−20.
(6) Heerman, L.; Tarallo, A. *J. Electroanal. Chem.* **1999**, *470*, 70−76.
(7) Mirkin, M. V.; Nilov, A. P. *J. Electroanal. Chem.* **1990**, *283*, 35−51.
(8) Cao, Y.; Searson, P. C.; West, A. C. *J. Electrochem. Soc.* **2001**, *148*, C376−C382.
(9) Scharifker, B. R.; Mostany, J.; Palomar-Pardave, M.; Gonzalez, I. *J. Electrochem. Soc.* **1999**, *146*, 1005−1012.
(10) Nagy, G.; Denuault, G. *J. Electroanal. Chem.* **1997**, *433*, 175−180.
(11) Nagy, G.; Sugimoto, Y.; Denuault, G. *J. Electroanal. Chem.* **1997**, *433*, 167−173.
(12) Fransaer, J. L.; Penner, R. M. *J. Phys. Chem. B* **1999**, *103*, 7643−7653.
(13) Oskam, G.; Vereecken, P. M.; Searson, P. C. *J. Electrochem. Soc.* **1999**, *146*, 1436−1441.

(14) Radisic, A.; Long, J. G.; Hoffmann, P. M.; Searson, P. C. *J. Electrochem. Soc.* **2001**, *148*, C41−C46.
(15) Fichthorn, K. A.; Weinberg, W. H. *J. Chem. Phys.* **1991**, *95*, 1090−1096.
(16) Atkins, P. W.; De Paula, J. *Physical Chemistry*, 7th ed.; W. H. Freeman: New York, 2002.
(17) Hoffmann, P. M.; Radisic, A.; Searson, P. C. *J. Electrochem. Soc.* **2000**, *147*, 2576−2580.
(18) Oskam, G.; Searson, P. C. *J. Electrochem. Soc.* **2000**, *147*, 2199−2205.
(19) Budevski, E.; Staikov, G.; Lorenz, W. J. *Electrochemical Phase Formation and Growth: An Introduction to the Initial Stages of Metal Deposition*; VCH: Weinheim, Germany, 1996.
(20) Scherb, G.; Kolb, D. M. *J. Electroanal. Chem.* **1995**, *396*, 151−159.
(21) Vereecken, P. M.; Strubbe, K.; Gomes, W. P. *J. Electroanal. Chem.* **1997**, *433*, 19−31.
(22) Quickenden, T. I.; Xu, Q. Z. *J. Electrochem. Soc.* **1996**, *143*, 1248−1253.
(23) D'Ajello, P. C. T.; Munford, M. L.; Pasa, A. A. *J. Chem. Phys.* **1999**, *111*, 4267−4272.
(24) Chyan, O.; Arunagiri, T. N.; Ponnuswamy, T. *J. Electrochem. Soc.* **2003**, *150*, C347−C350.
(25) Oskam, G.; Long, J. G.; Natarajan, A.; Searson, P. C. *J. Phys. D: Appl. Phys.* **1998**, *31*, 1927−1949.
(26) Hills, G. J.; Schiffrin, D. J.; Thompson, J. *Electrochim. Acta* **1974**, *19*, 657−670.
(27) Radisic, A.; West, A. C.; Searson, P. C. *J. Electrochem. Soc.* **2002**, *149*, C94−C99.
(28) Cao, Y.; West, A. C. *J. Electroanal. Chem.* **2001**, *514*, 103−108.